Neuro-Oncology Advances
5(1), 1–11, 2023 | https://doi.org/10.1093/noajnl/vdad133 | Advance Access date 12 October 2023

MRI phenotypes of glioblastomas early after treatment are suggestive of overall patient survival

Bárbara Schmitz-Abecassis, Linda Dirven, Janey Jiang, Jasmin A. Keller, Robert J. I. Croese, Daniëlle van Dorth, Rashid Ghaznawi, Ilse M.J. Kant, Martin J.B. Taphoorn, Matthias J.P. van Osch, Johan A.F. Koekkoek, and Jeroen de Bresser

C.J. Gorter MRI Center, Department of Radiology, Leiden University Medical Center, Leiden, The Netherlands (B.S.-A., J.A.K., D.D., M.J.P.O., J.B.); Medical Delta, South-Holland, The Netherlands (B.S.-A., M.J.P.O); Department of Neurology, Leiden University Medical Center, Leiden, The Netherlands (L.D., R.J. I.C., R.G., M.J.B.T., J.A.F.K.); Department of Neurology, Haaglanden Medical Center, The Hague, The Netherlands (L.D., R.J.I. C., M.J.B.T., J.A.F.K.); Department of Radiology, HagaZiekenhuis, The Hague, The Netherlands (J.J.); Clinical Artificial Intelligence Implementation and Research Lab (CAIRELab) and Department of Information Technology & Digital Innovation, Leiden University Medical Center, Leiden, The Netherlands (I.M.J.K.); Department of Digital Health, University Medical Center Utrecht, Utrecht, The Netherlands (I.M.J.K.)

Corresponding Author: MSc. Bárbara Schmitz-Abecassis, Department of Radiology, Leiden University Medical Center, C3-Q, Albinusdreef 2, 2333ZA Leiden, The Netherlands (b.schmitz_abecassis@lumc.nl)

Abstract

Background. Distinguishing true tumor progression (TP) from treatment-induced abnormalities (eg, pseudo-progression (PP) after radiotherapy) on conventional MRI scans remains challenging in patients with a glioblastoma. We aimed to establish brain MRI phenotypes of glioblastomas early after treatment by combined analysis of structural and perfusion tumor characteristics and assessed the relation with recurrence rate and overall survival time.

Methods. Structural and perfusion MR images of 67 patients at 3 months post-radiotherapy were visually scored by a neuroradiologist. In total 23 parameters were predefined and used for hierarchical clustering analysis. Progression status was assessed based on the clinical course of each patient 9 months after radiotherapy (or latest available). Multivariable Cox regression models were used to determine the association between the phenotypes, recurrence rate, and overall survival.

Results: We established 4 subgroups with significantly different tumor MRI characteristics, representing distinct MRI phenotypes of glioblastomas: TP and PP rates did not differ significantly between subgroups. Regression analysis showed that patients in subgroup 1 (characterized by having mostly small and ellipsoid nodular enhancing lesions with some hyper-perfusion) had a significant association with increased mortality at 9 months (HR: 2.6 (CI: 1.1–6.3); $P = .03$) with a median survival time of 13 months (compared to 22 months of subgroup 2).

Conclusions. Our study suggests that distinct MRI phenotypes of glioblastomas at 3 months post-radiotherapy can be indicative of overall survival, but does not aid in differentiating TP from PP. The early prognostic information our method provides might in the future be informative for prognostication of glioblastoma patients.

Key Points

- Distinct MRI phenotypes of glioblastomas at 3 months post-radiotherapy are significantly associated with overall survival.
- The same MRI phenotypes at 3 months post-radiotherapy do not seem to aid in differentiating between true- and pseudo-progression at 9 months after radiotherapy.

Importance of the Study

Determining brain MRI phenotypes of glioblastomas early after treatment can help in showing which combination of MRI markers is driving a lower survival chance 9 months after treatment. These distinct MRI phenotypes of glioblastomas could in the future guide complex clinical decision-making based on patient prognosis early after treatment assessment.

Glioblastoma is the most common and severe type of primary malignant brain tumor.[1] Current multimodal treatment after surgical resection includes radiotherapy and concomitant and adjuvant chemotherapy with temozolomide.[2] Despite this treatment, a high local recurrence rate is observed during the disease course (90%).[3] MRI is the cornerstone for brain tumor surveillance and aids clinicians in guiding management decisions. However, a challenge is that high-dose radiotherapy may cause treatment-induced abnormalities in the early stages after treatment (ie, pseudo-progression (PP)), which can look similar to tumor progression on conventional MRI scans.[2,4] Therefore, distinguishing between true tumor progression (TP) and PP early after treatment can be challenging. Early differentiation could aid clinicians in accurately identifying patients who require an alternative treatment strategy to delay further disease progression, and at the same time spare responding patients the burden of additional tumor-targeted treatment.

Structural MRI markers have shown some added value for identifying TP, specifically when assessing the size and the morphology of the enhancing lesion on post-contrast 3DT1 images.[5–8] Furthermore, several studies have shown that perfusion MRI (with dynamic susceptibility contrast [DSC] and/or arterial spin labeling [ASL]) has added value in distinguishing between TP and PP in glioblastomas.[9–15] However, despite perfusion MRI techniques being promising in differentiating between TP and PP, individual MRI markers showed at best only a modest association with tumor progression and overall survival. This indicates the need to combine MRI markers to get a more reliable early assessment of TP in glioblastomas[15].

More recently, a number of studies have focused on the use of radiomics in glioblastomas to analyze MRI markers in a combined way. One previous study found that structural MRI markers (gray-level texture markers) were associated with TP.[16] Few previous studies have specifically applied radiomics models on perfusion MRI with the aim of developing models that could accurately predict TP.[17–19] Moreover, radiomics approaches such as deep learning models rely on MRI markers of higher order that are not directly clinically translatable, and it is not always completely clear how these markers drive the algorithms decision-making (ie, which combination of MRI markers). With this in mind, we set out to explore an alternative approach, which includes grouping of patients with glioblastoma based on clinically scored structural and both ASL and DSC perfusion MRI markers.[20,21] We subsequently studied how these subgroups progressed over time. We have previously developed a method that was able to identify brain MRI phenotypes based on hierarchical clustering, which resulted in clinically meaningful sub-categories in other disease conditions. For example, we identified brain MRI phenotypes related to predisposition to postoperative delirium (in preoperative patients) and brain MRI phenotypes related to an increased risk of stroke and mortality (in patients with manifest arterial disease).[22] To date, it is unknown what specific MRI phenotypes exist in patients with a glioblastoma.

We hypothesize that MRI phenotypes of glioblastomas based on both structural and perfusion tumor characteristics early after treatment could help in the risk assessment of glioblastoma recurrence rate and overall survival time. We therefore aimed to establish brain MRI phenotypes of glioblastomas early after treatment by combined analysis of radiological scores of structural and perfusion tumor characteristics and to assess the relation of these phenotypes with tumor recurrence rate and overall survival time.

Materials and Methods

Patient Population

Patient clinical data were retrospectively retrieved from the clinical archive of the Leiden University Medical Center between the period of January 2015 and February 2022 following local IRB regulations. The study population consisted of adult patients with a histologically confirmed grade IV glioblastoma IDH wild-type or diffuse astrocytoma IDH-mutant, following the most recent WHO guidelines at the time of diagnosis. Consecutive patients who received post-operative treatment consisting of radiotherapy (in combination with concomitant and adjuvant chemotherapy), with at least a 3-month post-radiotherapy follow-up MRI scan with both ASL and DSC scans, and confirmation of TP or PP were included.

Tumor Progression and Survival Assessment

The diagnosis of TP or PP was based on the patients' medical charts including clinical and radiological findings discussed in the multidisciplinary team meetings at either 3, 6, and/or 9 months after radiotherapy. The diagnosis at each of the time points was scored on a 5-point Likert scale: (1) definite PP; (2) probable PP; (3) no preference; (4) probable TP; and (5) definite TP. The conversion to a binary scale was done by assessing scores 1 and 2 as tumor progression and 4 and 5 as no progression. In this way, the binary score agrees with clinical practice, that is, if there was doubt about the progression status (score of 3), treatment was continued (and assumed there was no progression). Updated molecular and pathological findings were leading

regarding the diagnosis in case of a re-resection. At the latest timepoint available (maximum of 9 months after radiotherapy), patients were only considered to have tumor progression if this was suggested by the clinical and radiological assessment, if the anti-tumor treatment regimen was changed, or if the patient was deceased.

Patient survival was calculated as the time between the start of tumor-targeted therapy (ie, the day of tumor surgical resection or biopsy) and the date of death.

Type of Surgical Resection

All patients underwent surgery for either maximally safe tumor removal (ie, total or partial resection of the enhancing part of the tumor) or a biopsy to obtain a histopathological diagnosis. Patients were considered to have had a total resection of the enhancing parts if no enhancing lesion was observed on the directly postoperative MRI scan (performed within 48 h after tumor resection). In contrast, if residual tumor enhancement was found on the directly postoperative MRI scan, it was considered a partial resection.

MRI Scans

Patients were scanned at approximately 3 months post-radiotherapy on a 3T MR scanner (Philips Ingenia or Achieva, Philips Healthcare, Best, The Netherlands). The MRI scans acquired followed the routine clinical guidelines for all scans collected, thus all imaging acquisition parameters reported are based on standard clinical practice. These included a post-gadolinium contrast-enhanced 3DT1 scan with 3D-TFE readout and T2-FLAIR scan, acquired with the following parameters: 3DT1: TR = 9.91 ms, TE = 4.67 ms, resolution = 1 × 1 × 1mm, field of view (FOV) = 220 × 175 × 156 mm, 0.3 ml per kg bodyweight of gadolinium-based contrast agent (gadoterate meglumine) and T2-FLAIR: TR = 11 000 ms, TE = 125 ms, resolution = 0.4 × 0.4 × 5.5 mm, FOV = 220 × 175 mm. During the period of data collection, changes to the ASL protocol were made, including transitioning from a 2D to 3D pCASL having changed the label duration (LD) and post-label duration (PLD). For 2D pCASL, LD = 1650 ms and PLD = 1525 ms (first slice) and 2120 ms (last slice). Whereas for the 3D pCASL both LD and PLD were 1800 ms. The remainder of parameters included resolution (2D/3D) = 3 × 3 mm/4 × 4 mm, slice thickness (2D/3D) = 7 mm/6 mm, FOV = 240 × 240 mm. Finally, the DSC scans were acquired with a SE-EPI sequence with the following parameters, TE = 75 ms, TR = 1600 ms, resolution = 2.6 × 2.3 × 5 mm, FOV = 240 × 210 mm; a third of the contrast agent was injected as pre-bolus.

Radiological Scoring of the Brain MRI Scans

An independent neuroradiologist scored the structural brain scans, that is, the contrast-enhanced 3D T1 and the T2-FLAIR scans of the 3 months postradiotherapy visit (and in doubt consulted a second experienced neuroradiologist for consensus), to determine (1) whether the tumor contrast enhancing lesions were either nodular or patchy on the contrast-enhanced 3D T1, (2) the presence of T2 hyperintense areas surrounding the enhancing lesion on the T2-FLAIR, and (3) the size of the tumor contrast enhancing and T2 hyperintense area in 3 orthogonal directions. The T2 hyperintense area was defined as the confluent hyperintense signal surrounding the contrast enhancing lesion, excluding any resection cavities. The measurements in 3 orthogonal directions were used to estimate the tumor volume for the contrast enhancing lesions and T2 hyperintense areas individually, as well as to calculate the shape as the eccentricity factor (EF). The volume was calculated using an ellipse formula, as this has been shown to correlate well with the absolute tumor volume, using the following formula[23]:

$$\frac{4}{3}\pi D1\,D2\,D3$$

where $D1$, $D2$, and $D3$ correspond to the sagittal, coronal, and axial measurements, respectively. The resulting volume was afterward converted to milliliters for the final volume calculation. The EF was calculated according to the following formula:

$$EF = \sqrt{1 - \left(\frac{PPD}{MD}\right)^2}$$

where MD is the maximal diameter (highest value in all 3 directions) and PPD is the largest perpendicular diameter, that is, the largest diameter in the other 2 directions.[24]

Tumor lesion perfusion was scored qualitatively using the contrast-enhanced 3DT1 and the T2-FLAIR as anatomical references. On the DSC relative cerebral blood volume (rCBV) maps were scored as either increased (hyper-perfusion), decreased (hypo-perfusion), or no change (iso-perfusion) compared to contralateral normal tissue. The ASL was scored as hyper-perfusion or iso-perfusion compared to the contralateral side, since hypoperfusion on ASL scans is especially difficult to identify.[25] Perfusion scores for both contrast enhancing lesions and T2 hyperintense areas were separately determined. For the clustering analysis, if there was more than one lesion in a patient, the most aggressive tumor contrast enhancing lesion and related T2 hyperintense area were included per patient. The lesion with the largest volume, increased perfusion and most nodularity was considered to be the most aggressive. In total, 23 radiological tumor markers were included (see the Supplementary Methods). These markers were rigorously selected to be the most representative to avoid overfitting and selection bias of the model.

Statistical Analysis

Hierarchical clustering analysis.—To identify different brain MRI phenotypes at 3 months post-radiotherapy, hierarchical clustering was performed on the available patient data consisting of the radiological structural and perfusion tumor characteristics. The visually scored markers were included in the model as either binary, categorical, or continuous variables. Continuous markers that did not have a normal distribution, including the volume and eccentricity, were normalized by multiplying by 100 and natural log-transforming, and thereafter normalized into z-scores. The normalization step allowed all markers to be equally scaled and then weighted by the analysis model.

Hierarchical clustering was performed using the Ward's method, Nbclust,[26] factoextra,[27] cluster,[28] and dendextend[29] in R version 4.1.2 (R Core-Team 2021). Initially, the model considers each patient as an individual cluster after which it tries to iteratively merge the 2 closest clusters while equally weighing each marker (ie, merge the clusters that share the highest number of markers in common; the agglomerative approach). In this way, the clustering analysis is performed in a hierarchical manner. Each time subclusters are merged into one cluster, the distance between the remaining clusters is subsequently updated in the model, and the next iteration starts. Ultimately, when all clusters have been merged only one cluster will remain. To determine the optimal number of clusters from the hierarchical clustering analysis, we used the heatmap and Dunn index. The Dunn index calculates the ratio of the smallest distance between markers within each cluster over the maximum distance between the clusters.

Differences between the subgroups with a different MRI phenotype of glioblastomas.—Descriptive statistics were used to describe the patient population. Clinical characteristics between the subgroups identified with the hierarchical cluster analysis were compared as follows: for categorical and binary variables, a chi-square test was used; continuous variables were compared using a one-way ANOVA or Kruskal-Wallis test, depending on the distribution of the tested variable. In order to assess how the subgroups differed from each other considering the different variables, Bonferroni post hoc analyses were performed for continuous variables and Bonferroni chi-square residual analyses for categorical variables.

Differences between the overall survival time of the subgroups.—A log-rank test was performed to determine whether the median overall survival times were significantly different between the different subgroups. For this, we compared the median overall survival times among subgroups 1, 3, and 4 and compared to the reference one, subgroup 2.

Association between different MRI phenotypes of glioblastomas and progression and survival.—First, a multivariable logistic regression analysis was performed to assess the association between MRI phenotype subgroups and TP. The model was corrected for age, KPS score, and surgical resection type. Whereas the first 2 variables were continuous, surgical resection type was categorized into 3 different groups (ie, biopsy, partial resection, and total resection).

Secondly, an adjusted Cox proportional hazard model was used to determine the association between the MRI phenotype subgroups and overall survival time. The model was corrected for age, KPS score, and surgical resection type. For sensitivity analysis, an unadjusted multivariable Cox proportional hazard model was performed to assess the influence of correcting for clinical variables on our results and thus to get more insight into the data. The subgroup chosen as a reference for the regression analysis had the least aggressive MRI markers (ie, subgroup 2). This subgroup with the least aggressive radiological markers was identified by an experienced neuroradiologist who assessed the structural and perfusion radiological markers of all subgroups (eg, hyper-perfusion and increased nodular enhancement were considered aggressive markers).

The threshold for significance was $P \leq .05$. All statistical analyses were performed using IBM SPSS version 25 (Chicago-IL).

Results

Patient Population

In total, 67 patients with a glioblastoma were eligible according to our inclusion criteria and were included in the analysis (Table 1). The majority (72%) had an isocitrate dehydrogenase (IDH)-wild-type tumor and most (61%) patients were male, with a mean age of 60 years (SD 13 years). Most patients (79%) had undergone total or partial resection, radiotherapy as well as concomitant and adjuvant chemotherapy, and a small group of patients were only treated with radiotherapy (21%). See Table 1 for all sociodemographic and clinical variables.

Representative examples of the scored MRI markers can be found in Figure 1, which includes perfusion markers characterized in ASL and rCBV maps as well as structural markers such as enhancing lesion patterns on contrast-enhanced 3DT1 and T2 hyperintense areas on T2-FLAIR.

Table 1. Baseline clinical characteristics of the patients with a glioblastoma.

Total number of patients included	67
Age (mean ± SD)	60 ± 13
Female	26 (39%)
Male	41 (61%)
IDH status	
Wild-type: glioblastoma	48 (72%)
Mutant: diffuse astrocytoma grade IV	5 (7%)
Unknown/ not determined*	14 (21%)
MGMT status	
Methylated	18 (27%)
Unmethylated	49 (73%)
KPS median (range)	90 (60–100)
Surgery type	
Total resection	31 (46%)
Partial resection	22 (33%)
Biopsy	14 (21%)
Radiotherapy (total dose)	
40 Gy	10 (15%)
45 Gy	10 (15%)
60 Gy	47 (70%)
Temozolomide chemotherapy	53 (79%)

*Cases diagnosed prior to WHO 2016 classification. IDH: Isocitrate dehydrogenase; MGMT: O6-methylguanine-DNA methyltransferase; KPS: Karnofsky Performance Scale.

Identification of Subgroups With a Different MRI Phenotype of Glioblastomas

The hierarchical clustering analysis resulted in the heatmap displayed in Figure 2. Establishing the optimal number of subgroups was a multistep process. First, we considered that with our number of patients included, the number of subgroups should be relatively low. Second, we inspected the heatmap (Figure 2) and found a good between-subgroup separation with 4 subgroups. Lastly, we considered the Dunn index, which also showed a relatively high value in 4 subgroups. The number of subgroups of patients with a different MRI phenotype of glioblastomas was therefore determined at 4 (with n = 12, 13, 17, and 25 patients in the subgroups respectively).

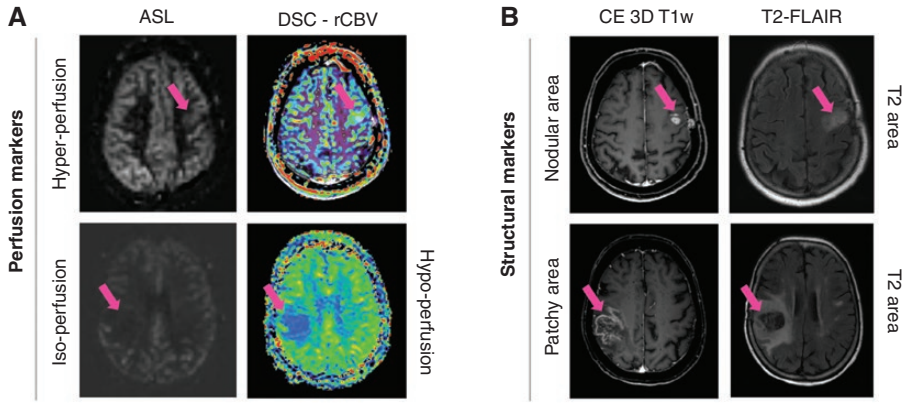

Figure 1. Examples of some of the MRI markers scored by a neuroradiologist. (A) Perfusion MRI markers retrieved from corresponding images, namely ASL and DSC-rCBV maps. On the upper and lower row examples of patients with increased and no change/decreased perfusion, for ASL and DSC respectively. In (B) contrast enhanced (CE) 3DT1 and T2-FLAIR MRI scans from which the structural markers were assessed; it shows examples of nodular and patchy contrast-enhancing areas, as well as T2 hyperintense areas. The scans on each row correspond to one patient.

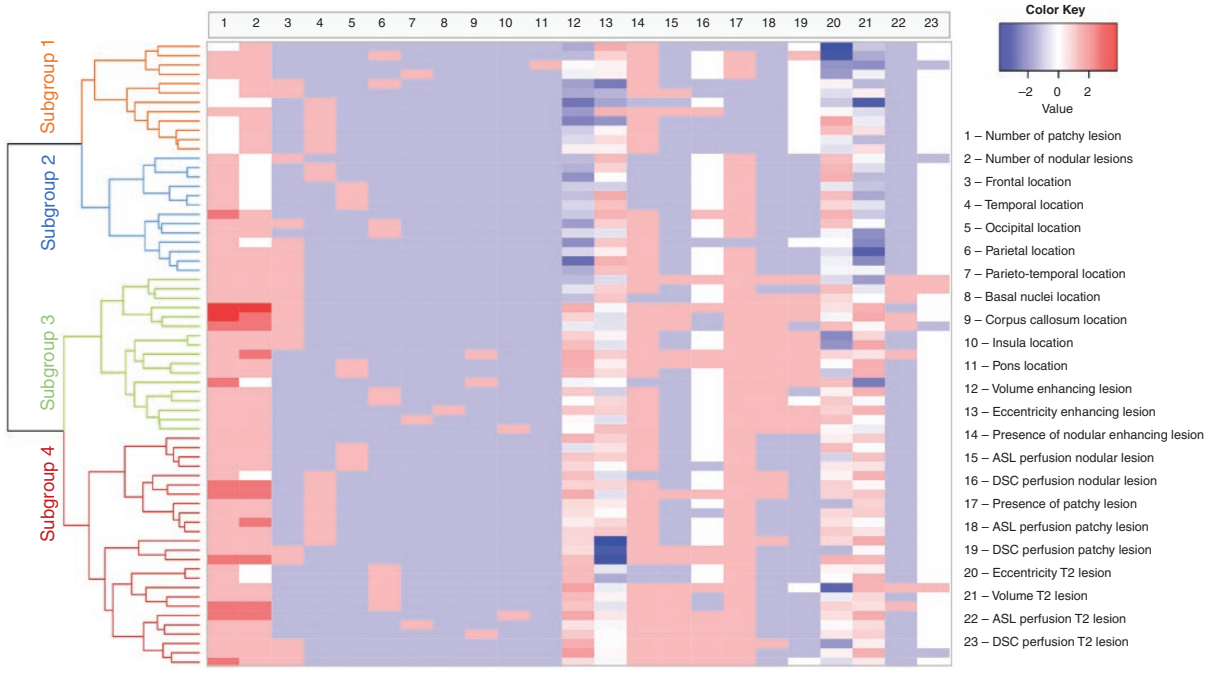

Figure 2. Heatmap results of the hierarchical clustering analysis. The subgroups (subgroup 1 (n = 12), subgroup 2 (n = 13), subgroup 3 (n = 17), and subgroup 4 (n = 25)) are represented in different colors on the left side of the figure. Each row represents one patient and each column represents one MRI marker. In total 23 MRI markers were included. The normalized values were included, where blue represents a low value and red a high value of the MRI marker.

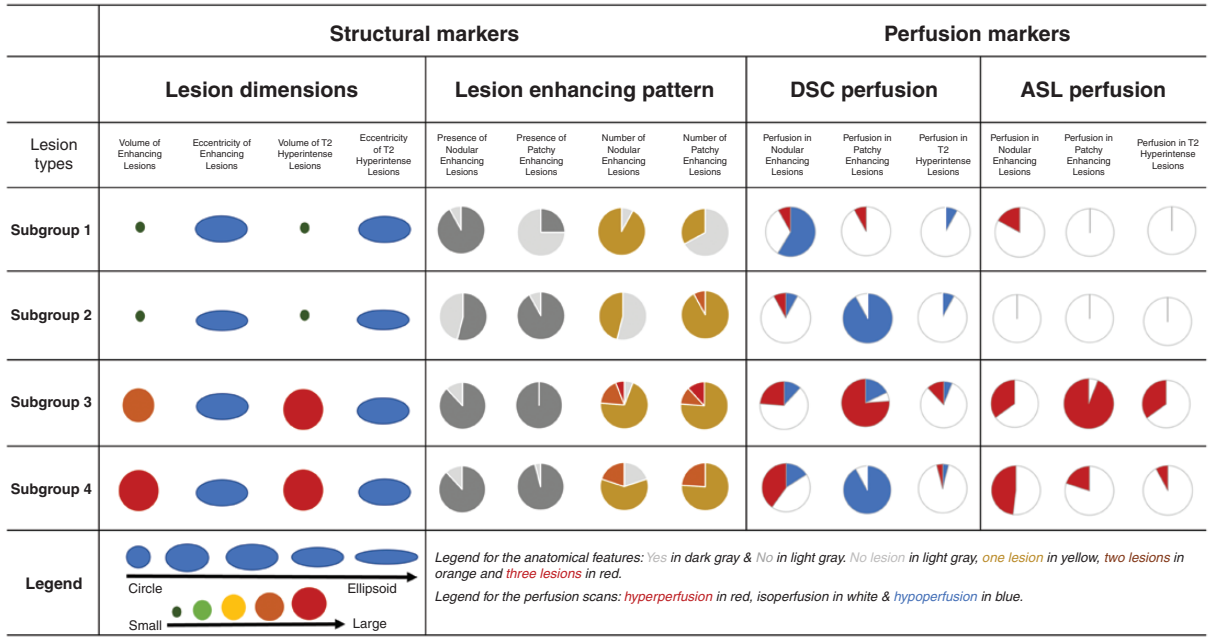

Figure 3. Illustration of the most representative structural and perfusion MRI markers as well as tumor volume and shape markers, per subgroup. These illustrative results are based on the values in Supplementary Table S2.

Differences Between the Subgroups with a Different MRI Phenotype of Glioblastomas

A summary of the clinical characteristics of these patient subgroups can be found in Supplementary Table S1. There were no significant differences between subgroups regarding KPS score, radiotherapy dose received, gender, IDH status, MGMT promotor methylation status, and receiving combined chemoradiotherapy (all $P > 0.05$). However, there was a significant difference in age and type of surgery between the 4 subgroups ($P = .013$ and $P = 0.001$ respectively). From the Bonferroni post hoc analyses it was evident that the overall significant difference in age was particularly observed because patients in subgroup 3 were significantly older than in subgroup 1 (68 vs 54 years, respectively, $P = .02$). For surgery type, subgroup 1 had significantly more total resections compared to subgroup 3 (75% vs 12%, respectively, $P = .003$) and subgroup 4 (75% vs 12%, respectively, $P = 0.001$), explaining the overall significant difference. Supplementary Table S2 shows the distribution of the MRI markers present in each subgroup. Regarding tumor location, the temporal tumor region was the only location that differed significantly between the subgroups, with more patients having a temporal lesion in subgroup 1 (50% vs 15%, 0%, and 32% in groups 2, 3, and 4, $P = .02$). As expected, the majority of all other MRI markers were significantly different between the resulting subgroups (all $P < .05$; Supplementary Table S2). The structural MRI markers that differed significantly between subgroups include the presence of a patchy enhancing lesions, the number of nodular and enhancing lesions, as well as the volume and eccentricity from both enhancing and T2 hyperintense tumor lesions ($P < .05$; Supplementary Table S2). Moreover, the perfusion markers differed significantly between subgroups, such as the DSC-rCBV for both nodular and patchy enhancing lesions, and the ASL-CBF of the nodular and patchy enhancing lesions and of the T2 hyperintense tumor areas ($P < .05$; Supplementary Table S2).

Overall, subgroup 1 was characterized by relatively few, small, and mostly nodular enhancing lesions with a more ellipsoid shape and some lesions showing hyper-perfusion. Subgroup 2 was characterized by relatively few, small lesions with mostly patchy enhancing lesions, with a more ellipsoid shape and almost no lesions with hyper-perfusion. Subgroup 3 had the most lesions and also had the highest volume and highest amount of lesions with hyper-perfusion. Lastly, subgroup 4 was characterized by a relatively moderate amount of nodular and patchy enhancing lesions with a relatively high volume, ellipsoid shape, and moderate amount of lesions with hyper-perfusion. A summary of the most relevant MRI markers of the MRI phenotypes of glioblastomas can be found in Figure 3

Differences Between the Overall Survival Time of the Subgroups

A significant difference was found between the overall survival times of the reference subgroup (subgroup 2) and subgroup 3 ($P = .009$), but not between the reference subgroup and subgroup 1 ($P = .166$) and 4 ($P = .191$; Supplementary Table S5, Supplementary Figure S3).

Association Between Different MRI Phenotypes of Glioblastomas and Progression and Survival

Out of the 67 patients, 49 showed a final diagnosis of TP at 9 months follow-up. Per subgroup this translated in

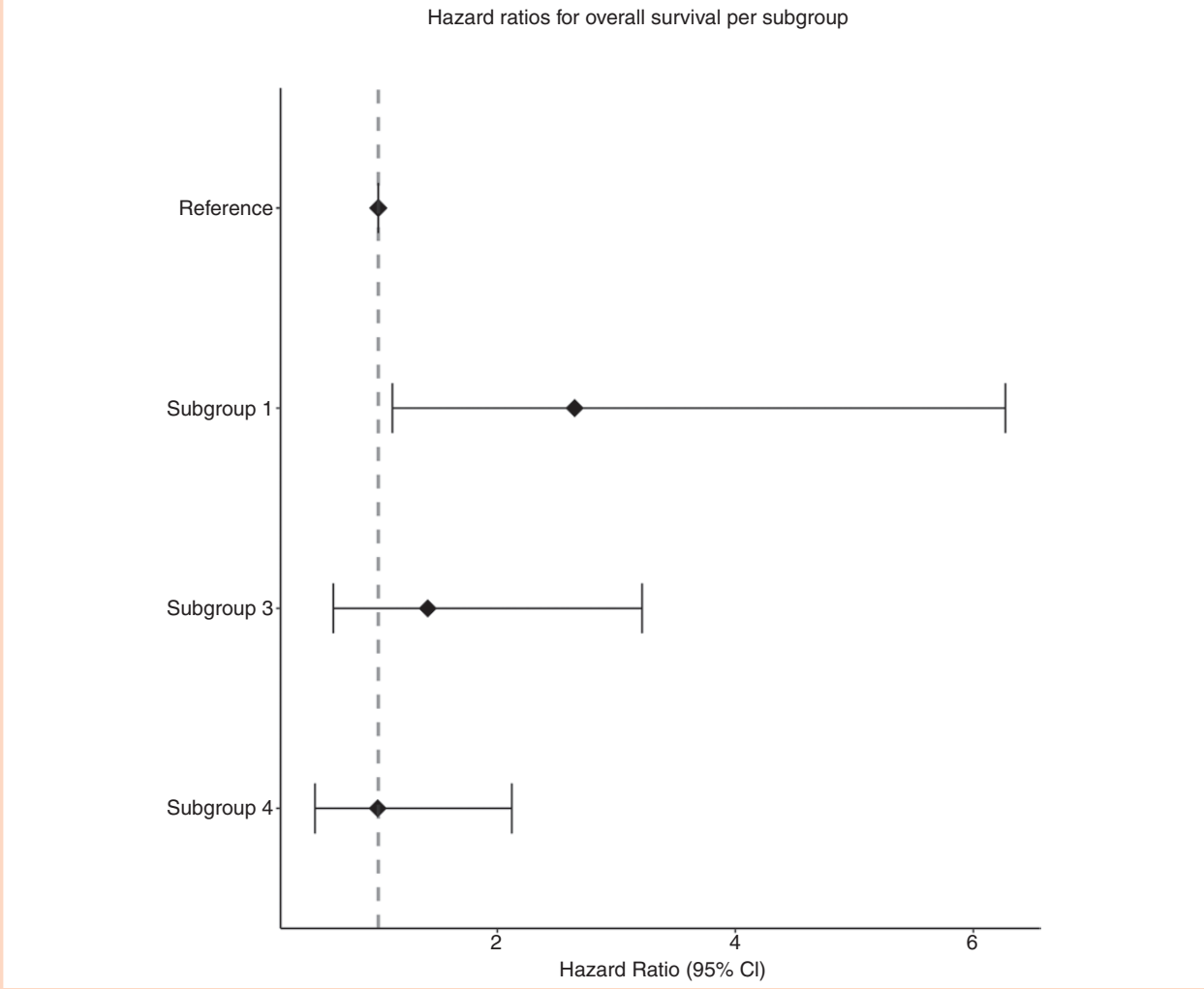

Figure 4. Forrest plot of the hazard ratios (95%-CI) per subgroup for survival. Illustrated results of the Cox proportional hazards survival analysis are shown (adjusted for age, KPS, and surgery type). Subgroup 2 has been set as a reference and marked with the striped line. Hazard ratios are shown with a 95% CI.

8/12 (67%) patients having TP in subgroup 1, 9/13 (69%) in subgroup 2, 14/17 (82%) in subgroup 3, and 18/25 (72%) in subgroup 4. From the multivariable logistic regression analysis, we found that subgroups 1 (HR: 1.3 (95% CI: 0.2–6.8); $P = .772$), 3 (HR: 1.7 (95% CI: 0.3–10.4); $P = .570$) and 4 (HR: 1.6 (95% CI: 0.3–8.4); $P = .551$) were not significantly associated with TP, compared to the reference subgroup 2 (Supplementary Table S6).

In total, 65 out of the 67 (97%) patients had passed away by the time the database was locked. The median survival in months per subgroup (with respective inter-quartile ranges) was: subgroup 1 = 13 (10–21) months, subgroup 2 = 22 (15–29) months, subgroup 3 = 11 (7–14) months, and subgroup 4 = 10 (8–18) months. Figure 4 shows the results of the survival analyses where subgroup 2 was taken as the reference group. Our results show that subgroup 1 (HR: 2.6 (95% CI: 1.1–6.3); $P = .03$) is significantly associated with mortality (Figure 5, Supplementary Figure 2), but not subgroups 3 and 4, when correcting for clinical variables (model 2). On the other hand, our secondary analysis included in the uncorrected logistic regression analysis, showed that subgroup 3 had a significant association with mortality (HR: 2.4 [95% CI: 1.1–5.0; $P = .03$]), but not subgroups 1 and 4.

Discussion

We identified distinct brain MRI phenotypes of glioblastomas in patients early after radiotherapy (at 3 months). Based on these brain MRI phenotypes we were able to define 4 distinct subgroups that also differed in their overall median survival times, but showed no differences in TP and PP rates.

In our current study, to establish different brain MRI phenotypes of glioblastomas, our clustering model hierarchically stratified the different patients based on the similarities between radiological MRI markers. Furthermore, we independently assessed the clinical outcomes. This

approach, contrary to most traditional machine learning models, is seen as a form of unsupervised learning. One of the advantages of our method includes the possibility of independently establishing new MRI marker combinations that in machine learning methods could otherwise not be determined.

The radiological MRI markers utilized in our study were based on radiological scoring of structural and perfusion images, and when combined, resulted in phenotypes of glioblastomas. Most of the MRI markers differed significantly between the 4 subgroups, and we identified subgroup 1 to have a significant association with mortality at 9 months. This subgroup's MRI phenotype of glioblastomas was characterized by relatively few, small, and mostly nodular-enhancing lesions with a more ellipsoid shape and some lesions showing hyper-perfusion, especially on ASL images, and the T2 hyperintense area on the DSC scans showed mainly hypo-perfusion. Some individual MRI markers that drive the model and that could influence the lower chance of overall survival in subgroup 1 can be identified. For example, the morphology of the nodular enhancing lesions are thought to reflect a more malignant phenotype.[30] Furthermore, the more ellipsoid shape of the lesions in subgroup 1 could indicate a more aggressive pattern of tumor infiltration in the neighboring healthy brain tissue.[31] Given the complexity of glioblastomas, and the uncertainty of what exact combination of MRI markers drives its severe prognosis, MRI phenotypes of glioblastomas can give more prognostically meaningful information and maybe in the future could help in treatment decisions.

Previous machine learning approaches have studied diagnostic performance using radiomics markers in brain gliomas.[20,21] For instance, a previous study utilized higher-order texture and gray-level intensity markers from ASL and DSC perfusion-weighted images and compared their quantitative patterns between high-grade and low-grade gliomas to assess diagnostic performance.[20] Radiomics in ASL and DSC were shown to be valuable, providing quantitative patterns to classify low and high-grade gliomas with an area under the curve of 0.888 and 0.962, respectively.[20] Similarly, another previous study also investigated if, among others, gray-level intensity and texture markers retrieved from DSC perfusion images, could identify glioma grades and IDH status. This study demonstrated stratification of glioma grades and IDH mutation status based on the DSC perfusion markers in a radiomics model performed correctly in 71% and 53% of the cases, respectively.[21] Both of these previous studies showed that a machine learning approach with MRI perfusion markers showed the potential to reliably classify gliomas grades and molecular genotypes. In traditional machine learning approaches, markers of interest were pre-determined and coupled to a known outcome for predictive modeling, where the markers of interest are mostly abstract and of higher-order, not directly representing clinical MRI markers. However, the main disadvantage of these machine learning approaches is that it is not always clear which exact marker (or combination of markers) is associated with a certain clinical outcome. Contrarily, in the current study we did not train a model to predict a certain outcome. Rather, we are utilizing MRI markers that are more representative of clinical radiological markers, and group the patients according to how similar these markers are. After this grouping, post hoc analyses are performed to gain insight into which combination of these markers (MRI phenotypes of glioblastomas) are underlying specific clinical outcomes. Utilizing phenotypes (ie, a combination of markers) instead of single markers can be more advantageous because it allows identification of which group of characteristics could be prognostically more meaningful in a disease with a complex biology. In this way, our approach is unique and also allows for a more comprehensive link between phenotype and outcome, as was also shown in previous studies of our group in other diseases.[22,32]

Regarding recurrence and overall survival outcomes of the 4 subgroups with a distinct MRI phenotype of glioblastomas, we observed different overall median survival times and TP cases. Subgroup 2 had the longest overall median survival time (22 months) and 69% of TP incidences. We found subgroup 1 to have a significant association with mortality at 9 months, while the percentage of TP cases (67%) was similar. These results were somewhat unexpected. The discrepancy between TP cases and overall survival time at 9 months follow-up could be explained by the large overall survival time range, a possible effect of a few outlier cases, and the small sample size for each subgroup. Moreover, subgroup 1 was shown to have a significant association with mortality at 9 months follow-up when correcting for confounding variables, including age.[33] This suggests that such a significant association observed in subgroup 1 is most likely a reflection of the tumor phenotype, not influenced by the age of the patients. When the model was not corrected for clinical variables, we found that only subgroup 3, with a considerably older median age (68 ± 11), had a significant association with mortality at 9 months. When comparing the median survival times, also not corrected for clinical confounders, a significant difference was also found for subgroup 3, as well as no significant difference for subgroups 1 and 4. The fact that clinical confounders are not weighted in most likely explains the non-significant findings, since both subgroups 1 and 4 have relatively short median survival times (compared to subgroup 2). An additional explanation for subgroup 4 could part from the crossing survival curves, which is probably due to a few outliers with longer survival times. Furthermore, we observed that patients with worse survival time in subgroups 3 and 4 (overall survival time of 11 and 10 months, respectively) not only had the lowest percentages of total resections (subgroup 3 and 4 = 12%) but also had the highest tumor volumes (subgroup 3 = enhancing lesion: 247.54 ml;T2 lesion: 1321.70 ml and subgroup 4 = enhancing lesion: 374.45 ml; T2 lesion: 1375.43 ml). This makes us believe that the subgroups not only reflect different tumor phenotypes but also the differences in surgical treatment. It is known that resection type is an important prognostic factor for survival, but does not correlate with the occurrence of TP or PP (similar to what we have observed in the present study).

In clinical practice, it is relevant to understand which demographic and disease-specific characteristics play a role in prognosis of the patient's disease. Since glioblastomas are known to recur, early assessment of tumor characteristics could better indicate patient prognosis on a

more personal level early after treatment. Contrary to traditional machine learning approaches, rather than helping predict an outcome, our study helps to understand which combination of radiological MRI markers are the imaging correlates of clinical outcomes, such as overall survival.[34] The early prognostic information our method provides might in the future be beneficial for prognosis of patients with a glioblastoma. More specifically, when assessing a patient's perfusion and structural tumor characteristics at 3 months, stratifying patients according to their MRI phenotype of glioblastomas could inform clinicians early on after treatment about the patient's outcome at 9 months. In order to further investigate the clinical impact, a larger study would need to be conducted, but our method shows promising results to justify and power such a study.

The strengths of our study include the well-characterized radiological MRI markers of glioblastomas, including DSC as well as ASL perfusion markers in combination with the extensive follow-up availability of both clinical and MRI data.[35] This allowed us to determine the clinical outcome of all patients considering both survival and progression. Furthermore, since ASL is not widely implemented in clinical imaging guidelines of glioblastomas, this dataset is unique for this patient population.[36]

Our study also has some limitations. A first limitation is that our sample size was limited to 67 patients. A reason for this was that glioblastoma patients who were certain to have died from non-tumor related causes or did not have structural and perfusion MR data available because of MRI contraindications were not included in our study. One of the evident consequences of our sample size is visible in the survival time ranges within subgroups. Our hierarchical clustering analysis approach could differentiate subgroups with primarily different radiological markers. These subgroups also showed to have different overall survival times. However, utilizing this approach for discriminating subgroups solely based on overall survival time is challenging. It could be interesting in the future to include a larger sample size and re-evaluate these findings. Although our selection procedure narrowed our patient population, it allowed us to be certain that the clinical outcome was related to their tumor diagnosis. Despite the relatively limited sample size, we were able to find clinically meaningful associations. A second limitation of our study is that the IDH status for some patients was unknown since some of the patients were diagnosed prior to 2016. This withheld us from including this variable in the survival and progression analyses, which would have been of added value since patients with an IDH mutation are known to have an overall better prognosis.[37] A third limitation is that over the years of data collection, the parameters of the ASL MRI acquisition changed. However, these changes were only minimal (applied to only one patient) and were not expected to have affected the visual perfusion scoring by the neuroradiologist in a significant way. Since the data used was retrospectively collected, the ASL acquisition parameters were set according to clinical standards, only including one PLD. Although including more PLD could make the images less sensitive to ATT artifacts, this is not yet the standard in clinical practice. The goal of our study was to also investigate how perfusion markers in such a hierarchical clustering model could be used to establish glioblastoma phenotypes. We strived to utilize the maximum number of markers representative of clinical practice, without being redundant. However, a larger number of markers or a different selection of markers, which would also be representative of other biological processes in the tumor, could provide more complete phenotypes of this disease. This could also lead to overlapping markers and therefore pruning the model to these overlapping markers. It would be interesting to see the results of future studies which would, for instance, also include metabolic information derived from MR spectroscopy or chemical exchange saturation transfer. Lastly, the ratings of the MRI scans were performed by one experienced neuroradiologist who consulted a second experienced neuroradiologist when in doubt to obtain consensus. Using only limited raters could be perceived as a limitation. However, we chose to invest in the quality of the raters instead of the quantity of the raters to achieve high-quality data.

In conclusion, we were able to establish 4 subgroups based on distinct brain MRI phenotypes of glioblastomas at 3 months post-radiotherapy. Our study suggests that these distinct MRI phenotypes of glioblastomas can be indicative of overall survival. The early prognostic information our method provides might be informative for prognosis in patients with a glioblastoma.

Supplementary material

Supplementary material is available online at *Neuro-Oncology* (https://academic.oup.com/neuro-oncology).

Keywords

glioblastoma | MRI | perfusion | tumor progression

Funding

This work was funded by Medical Delta Cancer Diagnostics 3.0 program.

Conflict of interest statement

None declared.

Authorship statement

B.S.A.: conceptualization, data curation, data analysis, statistical analysis, writing—original draft. L.D.: statistical analysis, writing—review and editing. J.J.: data collection and writing—review and editing. J.A.K.: data analysis, statistical analysis, writing—review and editing. R.J.I.C.: data collection and writing—review and editing. D.D.: data

curation and writing—review and editing. R.G.: statistical analysis and writing—review and editing. I.M.J. K.: methodology and writing—review and editing. M.J.B. T.: writing—review and editing. M.J.P. O.: conceptualization, funding, and writing—review and editing. J.A.F. K.: data collection and writing—review and editing. J. B.: Conceptualization, methodology, data curation, and writing—review & editing.

References

1. Louis DN, Perry A, Wesseling P, et al. The 2021 WHO classification of tumors of the central nervous system: a summary. *Neuro Oncol*. 2021;23(8):1231–1251.
2. Verma N, Cowperthwaite MC, Burnett MG, Markey MK. Differentiating tumor recurrence from treatment necrosis: a review of neuro-oncologic imaging strategies. *Neuro Oncol*. 2013;15(5):515–534.
3. Sheikh S, Radivoyevitch T, Barnholtz-Sloan JS, Vogelbaum M. Long-term trends in glioblastoma survival: implications for historical control groups in clinical trials. *Neurooncol Pract*. 2020;7(2):158–163.
4. Fatterpekar GM, Galheigo D, Narayana A, Johnson G, Knopp E. Treatment-related change versus tumor recurrence in high-grade gliomas: a diagnostic conundrum - Use of dynamic susceptibility contrast-enhanced (DSC) perfusion MRI. *AJR Am J Roentgenol*. 2012;198(1):19–26.
5. Hansen MR, Pan E, Wilson A, et al. Post-gadolinium 3-dimensional spatial, surface, and structural characteristics of glioblastomas differentiate pseudoprogression from true tumor progression. *J Neurooncol*. 2018;139(3):731–738.
6. Gladwish A, Koh ES, Hoisak J, et al. Evaluation of early imaging response criteria in glioblastoma multiforme. *Radiat Oncol*. 2011;6(1):1–7.
7. Abel R, Jones J, Mandelin P, Cen S, Pagnini P. Distinguishing pseudoprogression from true progression by FLAIR volumetric characteristics compared to 45 Gy isodose volumes in treated glioblastoma patients. *Int J Radiat Oncol Biol Phys*. 2012;84(3):S275.
8. Le Fèvre C, Constans JM, Chambrelant I, et al. Pseudoprogression versus true progression in glioblastoma patients: a multiapproach literature review Part 2—radiological features and metric markers. *Crit Rev Oncol Hematol*. 2021;159(January):103230.
9. Wang YL, Chen S, Xiao HF, et al. Differentiation between radiation-induced brain injury and glioma recurrence using 3D pCASL and dynamic susceptibility contrast-enhanced perfusion-weighted imaging. *Radiother Oncol*. 2018;129(1):68–74.
10. Ye J, Bhagat SK, Li H, et al. Differentiation between recurrent gliomas and radiation necrosis using arterial spin labeling perfusion imaging. *Exp Ther Med*. 2016;11(6):2432–2436.
11. Jovanovic M, Radenkovic S, Stosic-Opincal T, et al. Differentiation between progression and pseudoprogression by arterial spin labeling MRI in patients with glioblastoma multiforme. *J Buon*. 2017;22(4):1061–1067.
12. Choi YJ, Kim HS, Jahng GH, Kim SJ, Suh DC. Pseudoprogression in patients with glioblastoma: added value of arterial spin labeling to dynamic susceptibility contrast perfusion MR imaging. *Acta Radiol*. 2013;54(4):448–454.
13. Rau MK, Braun C, Skardelly M, et al. Prognostic value of blood flow estimated by arterial spin labeling and dynamic susceptibility contrast-enhanced MR imaging in high-grade gliomas. *J Neurooncol*. 2014;120(3):557–566.
14. Ozsunar Y, Mullins ME, Kwong K, et al. Glioma recurrence versus radiation necrosis? A pilot comparison of arterial spin-labeled, dynamic susceptibility contrast enhanced MRI, and FDG-PET imaging. *Acad Radiol*. 2010;17(3):282–290.
15. Manning P, Daghighi S, Rajaratnam MK, et al. Differentiation of progressive disease from pseudoprogression using 3D PCASL and DSC perfusion MRI in patients with glioblastoma. *J Neurooncol*. 2020;147(3):681–690.
16. Chen X, Wei X, Zhang Z, et al. Differentiation of true-progression from pseudoprogression in glioblastoma treated with radiation therapy and concomitant temozolomide by GLCM texture analysis of conventional MRI. *Clin Imaging*. 2015;39(5):775–780.
17. Yan JL, Toh CH, Ko L, Wei KC, Chen PY. A neural network approach to identify glioblastoma progression phenotype from multimodal MRI. *Cancers (Basel)*. 2021;13(9):2006–2009.
18. Shim KY, Chung SW, Jeong JH, et al. Radiomics-based neural network predicts recurrence patterns in glioblastoma using dynamic susceptibility contrast-enhanced MRI. *Sci Rep*. 2021;11(1):1–14.
19. Kim JY, Yoon MJ, Park JE, et al. Radiomics in peritumoral non-enhancing regions: fractional anisotropy and cerebral blood volume improve prediction of local progression and overall survival in patients with glioblastoma. *Neuroradiology*. 2019;61(11):1261–1272.
20. Hashido T, Saito S, Ishida T. A radiomics-based comparative study on arterial spin labeling and dynamic susceptibility contrast perfusion-weighted imaging in gliomas. *Sci Rep*. 2020;10(1):1–10.
21. Sudre CH, Panovska-Griffiths J, Sanverdi E, et al. Machine learning assisted DSC-MRI radiomics as a tool for glioma classification by grade and mutation status. *BMC Med Inform Decis Mak*. 2020;20(1):1–14.
22. Jaarsma-Coes MG, Ghaznawi R, Hendrikse J, et al; Second Manifestations of ARTerial disease (SMART) Study group. MRI phenotypes of the brain are related to future stroke and mortality in patients with manifest arterial disease: The SMART-MR study. *J Cereb Blood Flow Metab*. 2020;40(2):354–364.
23. Le Fèvre C, Sun R, Cebula H, et al. Ellipsoid calculations versus manual tumor delineations for glioblastoma tumor volume evaluation. *Sci Rep*. 2022;12(1):1–9.
24. Schwartz LH, Colville JAC, Ginsberg MS, et al. Measuring tumor response and shape change on CT: Esophageal cancer as a paradigm. *Ann Oncol*. 2006;17(6):1018–1023.
25. Van Osch MJP, Teeuwisse WM, Van Walderveen MAA, et al. Can arterial spin labeling detect white matter perfusion signal? *Magn Reson Med*. 2009;62(1):165–173.
26. Charrad M, Ghazzali N, Boiteau V, Niknafs AN. An R package for determining the relevant number of clusters in a data set. *J Stat Softw*. 2014;61(6):1–36.
27. Kassambara A. Package "factoextra": Extract and Visualize the Results of Multivariate Data Analyses for R. 2020.
28. Rousseeuw P, Struyf A, Hubert M, Studer M, Roudier P. "Finding Groups in Data"': Cluster Analysis Extended." 2022.
29. Galili T. An R package for visualizing, adjusting and comparing trees of hierarchical clustering. *Bioinformatics*. 2015;31(22):3718–3720.
30. Pallud J, Capelle L, Taillandier L, et al. Prognostic significance of imaging contrast enhancement for WHO grade II gliomas. *Neuro Oncol*. 2009;11(2):176–182.
31. Curtin L, Whitmire P, White H, et al. Shape matters: morphological metrics of glioblastoma imaging abnormalities as biomarkers of prognosis. *Sci Rep*. 2021;11(1):1–11.
32. Kant IMJ, Slooter AJC, Jaarsma-Coes M, et al; BioCog consortium. Preoperative MRI brain phenotypes are related to postoperative delirium in older individuals. *Neurobiol Aging*. 2021;101:247–255.
33. Shieh LT, Ho CH, Guo HR, et al. Epidemiologic features, survival, and prognostic factors among patients with different histologic variants of glioblastoma: analysis of a nationwide database. *Front Neurol*. 2021;12(November):1–9.

34. Palpan Flores A, Vivancos Sanchez C, Roda JM, et al. Assessment of preoperative measurements of tumor size by MRI methods as survival predictors in wild type IDH glioblastoma. *Front Oncol*. 2020;10(September):1–12.
35. van Dijken BRJ, van Laar PJ, Smits M, et al. Perfusion MRI in treatment evaluation of glioblastomas: clinical relevance of current and future techniques. *J Magn Reson Imaging*. 2019;49(1):11–22.
36. Hirschler L, Sollmann N, Schmitz-Abecassis B, et al. Advanced MR techniques for preoperative glioma characterization: Part 1. *J Magn Reson Imaging*. 2023;57(6):1655–1675.
37. Songtao Q, Lei Y, Si G, et al. IDH mutations predict longer survival and response to temozolomide in secondary glioblastoma. *Cancer Sci*. 2012;103(2):269–273.